This paper should be cited as: Li, Z., Huang, D., Luo, S., Huang, W. & Tomás, R. 2024. Pullout Performance and Branching Effect of Radial Cables to Reinforce the Steep Fill–Bedrock Interfaces: Investigation of a Pullout Test and a Numerical Simulation. International Journal of Geomechanics, 24, 04024088, doi: 10.1061/IJGNAI.GMENG-8368

Pullout performance and branching effect of radial cables to reinforce the steep fill-bedrock interfaces: investigations of a pullout test and a numerical simulation

Zhao Li[1], Da Huang[2,*], Shilin Luo[3], Wenbo Huang[4], Roberto Tomás[5]

[1]Ph.D. Candidate, School of Civil and Transportation Engineering, Hebei Univ. of Technology, Tianjin 300401, China. Email: 202011601014@stu.hebut.edu.cn

[2]Professor, College of Geology Engineering and Geomatics, Chang'an Univ., Xi'an 710064, China. Email: dahuang@hebut.edu.cn

[3]Lecture, College of Civil Engineering, Changsha Univ., Changsha 410022, China. Email: rosilynn@cqu.edu.cn

[4]Ph.D. Candidate, School of Civil and Transportation Engineering, Hebei Univ. of Technology, Tianjin 300401, China. Email: 201811601008@stu.hebut.edu.cn

[5] Professor, Dpto. de Ingeniería Civil. Escuela Politécnica Superior de Alicante. Univ. de Alicante. P.O. Box 99. E-03080, Alicante, Spain. Email: roberto.tomas@ua.es

*Corresponding author: dahuang@hebut.edu.cn (Da Huang)

Abstract

Steep fill-bedrock interfaces usually appear in many filling soil infrastructures, such as airports, houses, and road embankments in mountainous areas, when the excavation of rock slopes is constrained. These interfaces are prone to be tensioned up to failure, which easily trigger landslide of fill slopes. The anchor system buried in the fill soil, named radial cable system, was proposed for effectively enhancing the stability of steep fill-bedrock interfaces. At the interface, the steel ropes of the anchor section cable are equally divided into three sub-cables with a radial distribution. The pullout performance, failure evolution, and branching effect of the radial cable coupled with anchor plates were studied by a pullout test (in a laboratory setup) and a numerical simulation. The results showed that (1) the ultimate pullout capacities (P_u) of the radial cables were 193.53–312.94 % (for

7 mm diameter of the anchor plate) and 141.25–247.50 % (for 10 mm diameter of the anchor plate) greater than that of the single cables; (2) the pullout performance of the radial cable was significantly improved with an increase in the diameter of the anchor plate; the optimal radial inclined angle of sub-cables coupled with anchor plates was 15°; (3) the soil surrounding the radial cable showed a progressive failure pattern, and its failure area was basically a symmetric conical; (4) the radial cable can better reinforce the steep fill-rock interface than the conventional cable, as verified by a hill-fill project. The results of this study provide some new and important guidelines about the design and application of the radial cable system.

Keywords

Radial cable; Pullout performance; Branching effect; Fill slope; Steep fill-bedrock interface

Introduction

Economic development and urbanization advancements have fostered the construction of airports, houses, roads, dams and other infrastructures in mountainous regions, such as those in Southwest China, Japan, Switzerland, Spain, and Turkey (Cao et al. 2011; Zhang et al. 2017; Bru et al. 2018; Murao et al. 2018; Ersoy et al. 2019; Carey et al. 2021). Complex mountainous topographies result in a large number of high fill slopes, especially for airport construction in mountainous area (Tong et al. 2014; Zhang et al. 2015; Zhao et al. 2019; Zhou et al. 2019). In recent years, both the number and height of the fill slopes have gradually increased with a maximum filling height exceeding 100 m in China (Li et al. 2022). The properties of both the fill and fill-bedrock interface control the stability of the fill slope (Li 2013; Eid et al. 2015; Cen et al. 2017). When the fill-bedrock interface is steep owing to the constraint imposed by the construction conditions, for instance, the existing buildings are located on the top of high and steep rock slopes, reducing the slope ratio through the excavation is impossible (Fig. 1). Furthermore, if the steep fill-bedrock interface is located on the upper part of the fill slope, the significant difference in the stiffness of both materials considerably reduces the tensile capacity of the interface (Fig. 1). Therefore, the interface is prone to be tensioned and opened, resulting in a combined slide-tension failure of the fill soil induced by the infiltration of rainwater or surface water along the open interface (Day 1992; Cen et al. 2017; Huang et al. 2019). This underlines the substantial importance of the reinforcement of the steep fill-bedrock interface, which controls the tensile deformation.

Cable systems can effectively resist the tensile load and ensure slope stability (Yang et al. 2015) and have been widely applied. To improve the pullout capacity and reinforcement effect of

anchoring systems, prior reports on cable system have mostly focused on the embedment depth (Dickin 1988; Dickin and Laman 2007), anchor spacing, anchor plates (i.e., the spacing, inclination angle, quantity and shape of anchor plates) (Yu et al. 2011; Liu et al. 2012; Bhattacharya and Kumar 2014; Evans and Zhang 2019; Tilak and Samadhiya 2021), soil properties (Dickin 1988; Rangari et al. 2013), long-term action (Chen et al. 2013; Xie et al. 2017; Shi et al. 2019), static and dynamic load conditions (Rangari et al. 2013; Zhou et al. 2019), etc. In addition, the reinforcement effect of anchor system can also be improved by increasing the strength and integrity of the soil around the anchor system (such as by adding geogrids, steel grids, fibers and other methods in the soil) (Sawwaf 2007; Hejazi et al. 2012; Lajevardi et al. 2013; Niroumand and Kassim 2013; Abdi and Zandieh 2014; Alam et al. 2014), developing new materials for the anchor system (He et al. 2014), and coupling with anti-slide piles or frame beam structures (Fu et al. 2018; Shi et al. 2019; Yan et al. 2019).

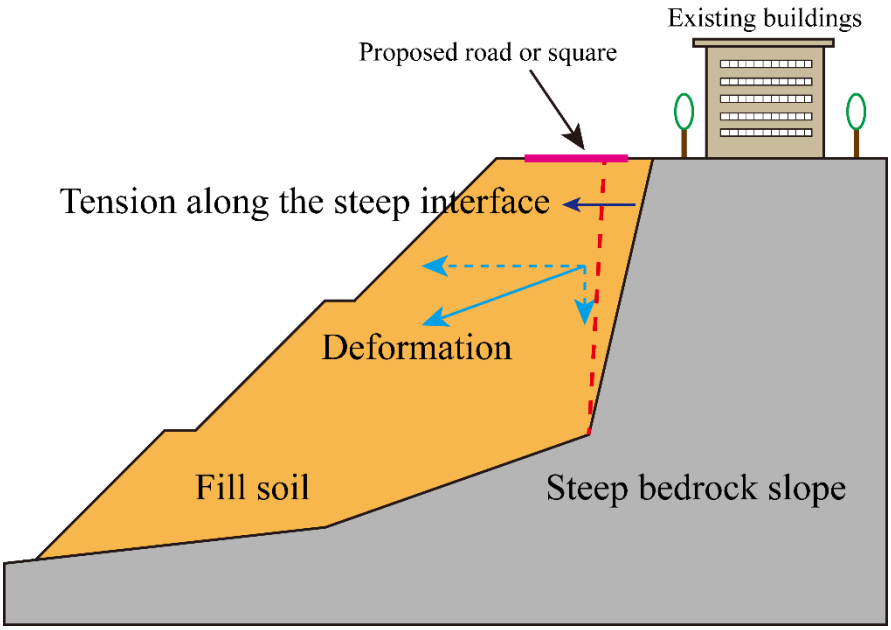

Fig. 1. Tensile deformation along the steep fill-rock interface at the upper part of a fill slope.

In short, the pullout capacity can be effectively increased based on the existing anchoring system

design methods and techniques mentioned above. Nonetheless, the pullout performances of the cable systems are poor when they are applied for reinforcing the steep fill-bedrock interface of the high-fill slopes (Huang et al. 2019). Therefore, the radial cable system for controlling the large horizontal deformation of fill slopes and preventing the separation of the fill from the steep fill-bedrock interface has been proposed (Huang et al. 2019). This system is characterized by its high pullout capacity, bonding capacity, and stiffness in the fill soil owing to its branching effect. In the previous study (Huang et al. 2019), a pullout test and a numerical study were used for investigating the pullout capacity of the radial cable with different radial inclined angles. However, the previous study did not consider the anchor plate, which is a significant part of the radial cable; and the failure process of the soil around cables was only analyzed by discrete-element method (DEM) simulations as the soil failure surface was fixed by the boundary of the model box (Huang et al. 2019). Consequently, the radial cable should be further investigated for overcoming the limitation of the previous study.

In this study, a series of pullout tests were conducted on radial cables coupled with anchor plates in a laboratory setup, and the pullout performance, branching effect, and failure evolution of the soil (around the cables) of the radial cable were explored. The pullout tests focused on evaluating the influence of radial inclined angle (β) and diameter of the anchor plate (D) on the pullout performance of the radial cable. In addition, the radial cable system was applied to an airport fill slope with a steep fill-bedrock interface in southwest China for verifying its reinforcement effects and exploring its mechanism to prevent landslide.

Radial cable system

The radial cable system is mainly composed of four parts (Fig. 2): (1) the anchorage section cable anchored in the bedrock, which provides the anchoring force (namely tensile resistance); (2) three sub-cables buried in the fill soil with a radial distribution, which are obtained by equally separating the steel ropes of the anchorage section cable at the steep fill-bedrock interface; (3) shear keys embedded above each radial cable, which can provide shear capacity along the interface and overcome the deficiency of the cables; (4) anchor plates at and short U-shaped rigid rods arranged on the sub-cables, which can increase the bonding force between the fill soil and sub-cables.

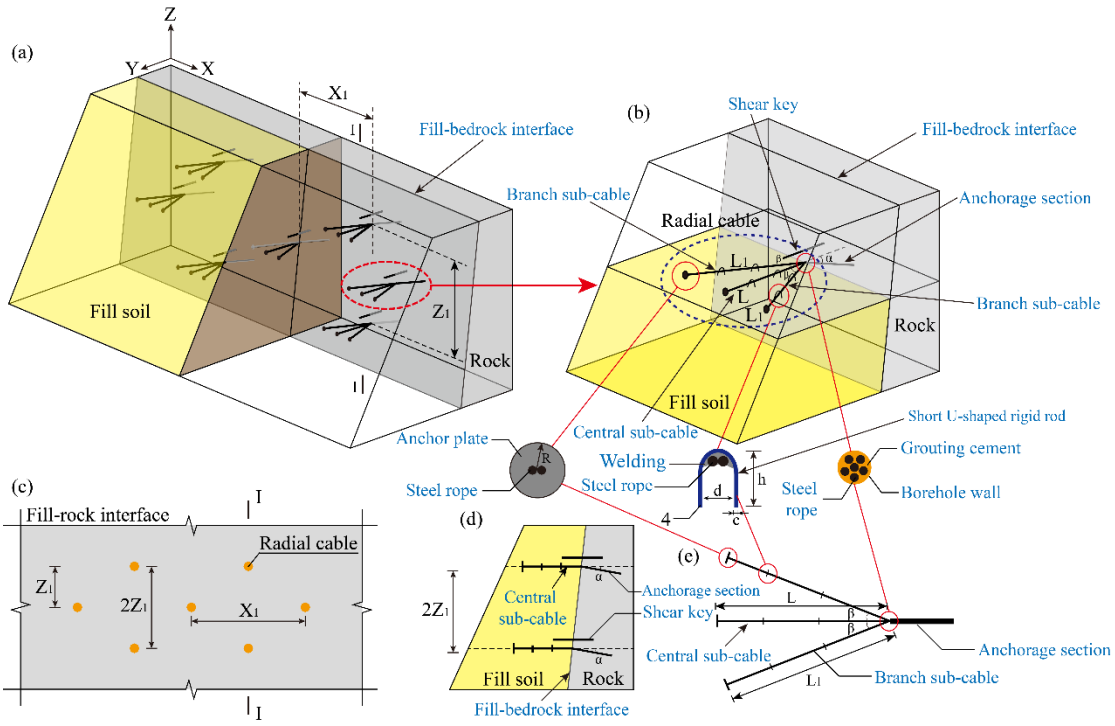

Fig. 2. Scheme of the radial cable system to reinforce steep fill-bedrock interfaces: (a) Three-dimensional scheme; (b) Local amplification for a radial cable; (c) Radial cable arrangement at the interface; (d) I-I cross-section; (e) Radial cable structure. (Modified from Huang et al. 2019).

To increase the overall pullout performance of the radial cable in the fill slope, the anchorage

section cable must consist of at least six steel ropes. The anchorage section cable is equally divided into one central sub-cable and two branch sub-cables at the interface (Fig. 2), and each sub-cable consists of at least two steel ropes. The central sub-cable is horizontally arranged in the direction of the borehole in the anchorage segment, and the branch sub-cables are spread in a symmetrical horizontal radial pattern with the central sub-cable as the central axis [Fig. 2(b) and Fig. 2(e)]. The branch sub-cables form an angle β with the central sub-cable to achieve branching effect.

To improve the pullout capacity of the anchorage segment and meet the grouting construction conditions, the inclination angle (α) of the anchorage borehole in the bedrock should not exceed 10° [Fig. 2(b) and Fig. 2(d)]. To increase the bonding force and prevent slippage between the sub-cables and fill soil, some short U-shaped rigid rods are used for fixing the sub-cables at equal intervals. The sub-cable is fixed at the central part of the short U-shaped bent section, and their rods are driven downwards into the fill soil [Fig. 2(b) and Fig. 2(e)]. Additionally, at least one anchor plate should be arranged at the end of each sub-cable. To facilitate the coordinated construction between anchoring and filling works, the radial cables are arranged in staggered rows in the fill slope [Fig. 2(c)–Fig. 2(d)]. The vertical spacing between adjacent rows (Z-direction in Fig. 2) is the fill layer thickness. The horizontal spacing of radial cables in the same row (X-direction in Fig. 2) should be slightly greater than L·sinβ (where L is the length of each sub-cable) for reducing the negative overlapping between adjacent sub-cables. After a layer of fill is constructed, a row of radial cables on the ground surface of the fill is arranged. This procedure is repeated until the top of the filling is reached. During the construction period between two layers of the fill soil, the constructed fill soil should be compacted by heavy hammer or rolling methods for strengthening the bonding force between the fill soil and sub-cables. The new radial cable system acts on the fill soil in a dendritic

or claw-shape manner, which effectively improves the pullout and shear capacity of the high and steep fill-bedrock interface and prevents the separation between the fill soil and bedrock surface. This system is simple in structure and convenient in construction of fill slope. Furthermore, the large-scale slope excavation of high and steep bedrock slopes can be avoided.

Scheme of the pullout test

Test equipment and materials

The test equipment of the pullout test is shown in Fig. 3. The length, width, and height of the model box were 1000, 400, and 560 mm, respectively. The model box was mainly welded using steel angles and plates, and a 10 mm thick tempered glass was used on one side of the box for observation [Fig. 3(a)]. During the pullout test, a vertical load was applied using the heavy load stacking method. The horizontal pullout load was provided by the threaded rod driven by the low-speed motor, which enabled flexible adjustment of the pullout rate according to the test requirements. Additionally, the test data was collected by a displacement sensor, load cell, and static strain gauge. The function of the clamp, as shown in Fig. 3, is to prevent the anchor cable from sliding during the pullout process and connect it with the load cell. Notably, the cable, fixture, load cell, threaded rod, and displacement gauge were located at the same level. Furthermore, noteworthily, the short U-shaped rigid rods were not considered in the physical model test.

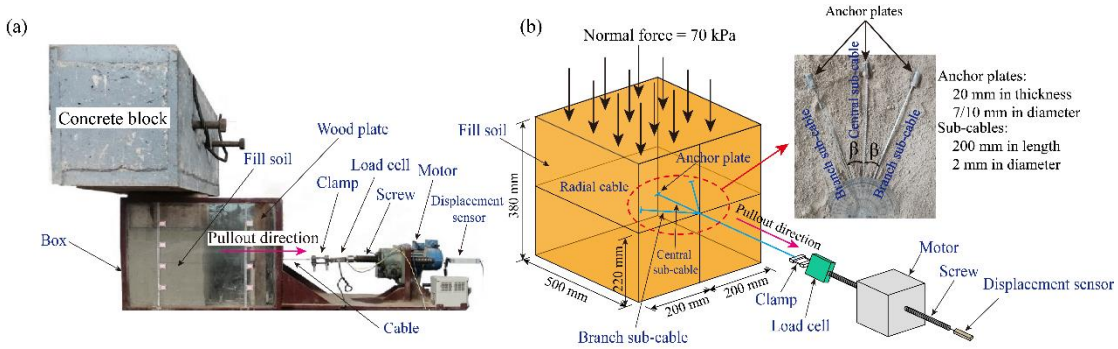

Fig. 3. Test models and devices: (a) Photo of the test devices; (b) Sketch of the test models.

A cohesive soil was used for simulating the fill material, and the particle gradation curve is shown in Fig. 4. The physical and mechanical parameters of the soil compacted under the identical conditions and the soil used in the pullout test are listed in Table 1. As shown in Fig. 3(b), the sub-cables of the radial cable buried in the fill soil were composed of three 200 mm length steel ropes with a diameter of 2 mm, and the radial inclined angle (β) between the central sub-cable and branch sub-cable was arranged. In addition, the rigid anchor plate was made of a steel bar, with 7 or 10 mm diameter and 20 mm thickness. The anchorage section cable was composed of three sub-cables bounded together by an aluminum clamp [Fig. 3(b)].

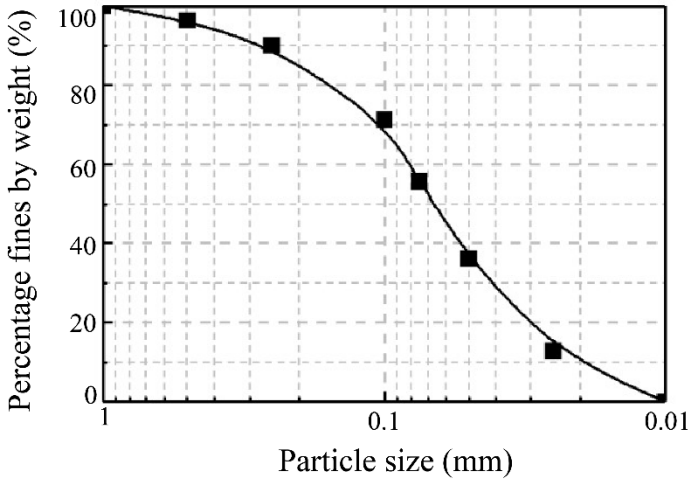

Particle size range (mm)	1 to 0.5	0.5 to 0.25	0.25 to 0.1	0.1 to 0.075	0.075 to 0.005	0.005 to 0.0025	0.0025 to 0.001	<0.001
Percentage fines by weigth (%)	3.55	6.39	18.85	15.57	19.40	23.50	12.29	0.45

Fig. 4. Particle distribution curve of the tested fill soil. Note: The particle gradation curve was tested by sieve analysis method and hydrometer method. The reference code is "Standard for geotechnical testing method (GB/T 50123-2019)".

Table 1. Physical and mechanical properties of tested fill soil.

Density (kg/m^3)	Cohesion (KPa)	Friction angle (°)	Elastic modulus (MPa)	Poisson's ratio	Dilatancy angle (°)	Moisture content (%)	Liquid limit (%)	Plastic limit (%)	Plasticity index
1890	15.8	27.5	125	0.3	3	3.5	40	19	21

Note: 1. The density was tested by ring knife method; The Cohesion, Friction angle, Elastic modulus, Poisson's ratio, Dilatancy angle were tested by triaxial compression test; The Moisture content was tested by drying method; The Liquid limit and Plastic limit were tested by liquid-plastic limit combined method; 2. The reference codes are "Standard for geotechnical testing method (GB/T 50123-2019)", "Code for investigation of geotechnical engineering (GB 50021-2001)" and "Code for design of building foundation (GB 5007-2011)".

Test procedure

A thin layer of grease was painted on the inwall of the model box before the soil was filled to reduce the effect of boundary conditions during the pullout test. The soil was compacted in 20 mm thick layers. During the filling process, the free surface of the soil was supported with a wood plate for preventing soil collapse.

When the soil was filled to a height of 220 mm, the radial cable anchorage section was fixed with the clamp, and then the clamp, load cell, and motor screw were connected in turn and the displacement gauge was fixed to the end of the screw (Fig. 3). Meanwhile, the reinforced section of the radial cables was buried in the soil, and the β of radial cables was set according to the test scheme. The central sub-cable was placed in the center of the soil along width direction, and the embedded length of each sub-cable was set to 200 mm. Subsequently, the filling was continued until the height of the soil was 380 mm. Furthermore, the final fill soil length and width were 400 and 400 mm, respectively (the volume was 0.0608 m^3). Then, the concrete block was placed on the top of the fill soil to apply a constant vertical load of 70 kPa, which was designed to simulate the buried depth of the cables in actual projects. Finally, the wood plate was dismantled to form a free surface after the fill soil had been compacted for 24 h under the gravity of concrete block, and the radial cable was pulled out with a pullout rate of 0.01 mm/s. As can be seen from the data listed in Table 2, the physical model test included two types of pullout tests of the single cable and radial cable with different D. Herein the single cable reinforcement section was buried at the same position as the central sub-cable of the radial cable.

Table 2. Parameters used for the configuration of the pullout test of the cables.

Number	Radial inclined angle β/ (°)	Anchor plate out diameter D/ (mm)	Anchor plate thickness H/ (mm)	Cable diameter d/ (mm)	Reinforcement length L/ (mm)	Vertical uniform load Q/ (KPa)
1	-	7	20	2	180	70
2	-	10	20	2	180	70
3	-	-	-	2	180	70
4	3	7	20	2	180	70
5	10	7	20	2	180	70
6	15	7	20	2	180	70
7	20	7	20	2	180	70
8	25	7	20	2	180	70
9	3	10	20	2	180	70
10	10	10	20	2	180	70
11	15	10	20	2	180	70
12	20	10	20	2	180	70
13	25	10	20	2	180	70

Note: Number 1 to 3 are the parameters used for the pullout test of the single cable; Number 4 to 13 are the parameters used for the pullout test of the radial cables.

Results of the pullout test

Results of the single cable

Pullout performance of the single cable

The curves (P-S curve) of the pullout force (P) versus anchor displacement (S) of a single cable with anchor plates (D=7 or 10 mm) and a single cable without anchor plate (D=0 mm) are shown in

Fig. 5. The P-S curves of the single cables exhibit a "saddle shape" and can be divided into four stages. Taking the P-S curve of the single cable with D=7 mm as an example for explaining the pullout process, the first stage (S-1) is the elastic stage (OA section), in which the pullout force linearly increases with the displacement. The second stage (S-2) is the elastic-plastic stage (AB section), which exhibits a continual slow increase in the pullout force, reaching the maximum value at point B (Fig. 5). The slope of the P-S curve of the AB section significantly decreased compared with the elastic stage. The third stage (S-3) is the softening stage (BC section). The surrounding soil started entering into a softening stage, and the pullout force slowly decreased with displacement. The fourth stage (S-4) corresponds to the failure stage (CE section). When the cable displacement reached the failure displacement (Point C), the pullout force sharply dropped to zero. Consequently, the cable was completely pulled out and lost its pullout bearing capacity.

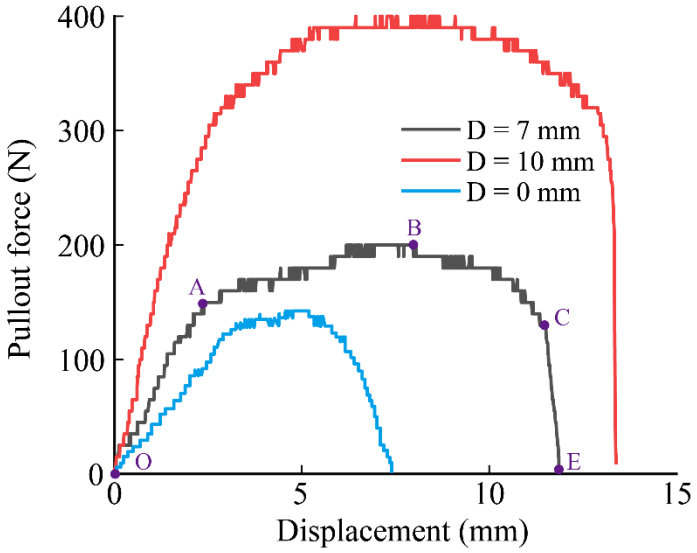

Fig. 5. Curves of the pullout force versus displacement of the tested single cables. Note: D is the diameter of the anchor plate.

As shown in Fig. 5, the pullout capacity (P_u) of the single cable without anchor plate was 143.00 N, whereas the P_u of the single cables coupled with the anchor plates were 201.00 N (D=7 mm) and

400.00 N (D=10 mm), which were 40.56 and 179.72 % greater than that of the single cable without anchor plate, respectively. During the softening stage, the displacement of the single cable without anchor plate was 2.10 mm, and the displacements of the single cables coupled with the anchor plate were 3.47 mm (D=7 mm) and 4.84 mm (D=10 mm), which were 65.63 and 130.25 % greater than the single cable without the anchor plate. This indicates that the single cable with the anchor plate can continue to bear the pullout force for a longer time under the identical working conditions. Therefore, it will take longer time and a larger displacement when the slope is damaged, which would allow prediction and early warning of the landslide of the fill slope. Additionally, the P_u and softening stage displacement of the single cable increased with D as the larger D extended the action range of the cables, and the surrounding soil could provide a greater pullout capacity, improving the pullout performance of the cable. Furthermore, the gradient of the P-S curves in the elastic stage enlarged with an increase in D (Fig. 5). This indicated the increase in D to be conducive to rapidly mobilizing the pullout capacity of the cables, and consequently, the pullout performance significantly improved in the elastic stage.

Failure process and final failure surface of the fill soil

The soil failure processes of single cables are similar to each other. Therefore, only the soil failure process around the single cable (D=7 mm) is described in detail in Fig. 6 (the red lines and green arrows in Fig. 6 represent soil cracks and pullout direction, respectively). The initial characteristics of the free face of the fill soil before pullout are shown in Fig. 6(a). For P=65 N, a fine vertical crack first appeared directly above the cable, with a length and width of approximately 80 and 3 mm, respectively [Fig. 6(b)]. For P=201 N, the fine crack in Fig. 6(b) gradually extended upwards to the

top of the free surface of the fill soil and eventually inclined through crack. Additionally, a new fine vertical crack also emerged below the cable; however, the new fine crack was shorter in length [Fig. 6(c)]. Subsequently, the fine crack beneath the cable gradually extended towards the bottom of the free surface more slowly than the upper crack. With the continuation of the pullout process, a large area suddenly collapsed in the free surface of the fill, and new cracks were developed on the failed surface. Meanwhile, a “conical” failure surface (Meyerhof 1968; Dyson and Rognon 2014; Evans and Zhang 2019), centered on the cable and radially extended along the cable, was initially formed [Fig. 6(d)–Fig. 6(e)]. When the pullout displacement exceeded the displacement of Point C, as shown in Fig. 5, a small volume of the soil collapsed near the cable. Subsequently, the depth of the failure surface slightly increased without an obvious variation in the shape of the “conical” soil failure surface [Fig. 6(f)].

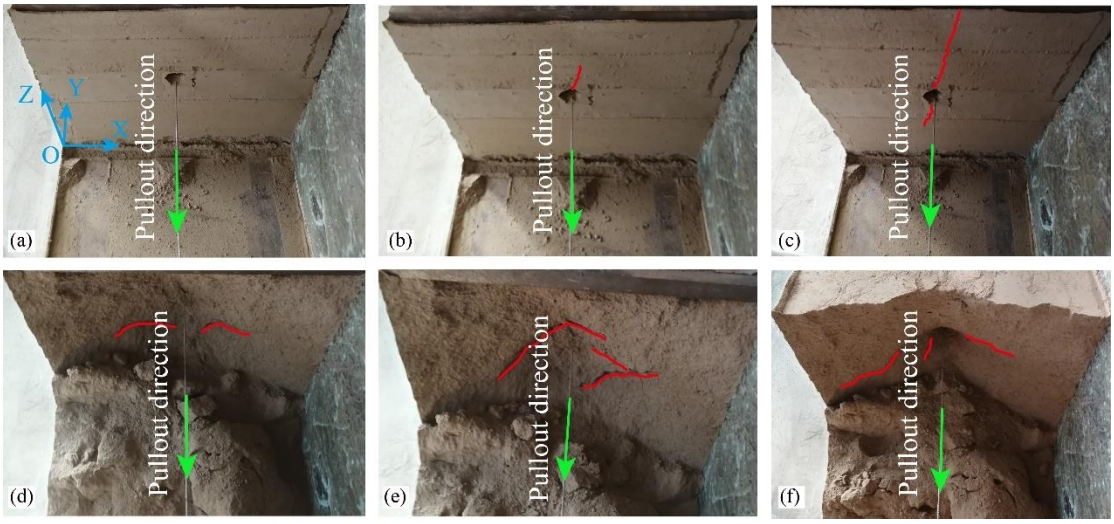

Fig. 6. Soil failure process under the pullout force of the single cable (D=7 mm): (a) P= 0 N (Point O in Fig. 5); (b) P=65 N (in the first stage); (c) P=201 N (Point B in Fig. 5); (d) P=190 N (in the third stage); (e) P=160 N (in the third stage); (f) P=5 N (Point E in Fig. 5).

The soil final failure surfaces and three-dimensional displacement contours of the final failure

surfaces of the single cables (D=7 and D=10 mm) are shown in Fig. 7. In contrast, the soil final failure surfaces for height between 0 and 50 mm could not be measured as the soil collapsed in the free face. Therefore, the height between 50 and 380 mm was selected for obtaining the three-dimensional displacement contours of the failure surfaces. The final failure surfaces were basically symmetrical on the left and right sides (X-direction) of the cable and approximated a “conical” pattern (Fig. 7) owing to the shear expansion of the fill soil and widened failure surface cause by the end-bearing effect of the additional anchor plates of the cables. The extent of the soil final failure surface increased with D, as the larger D increased the force range of the soil causing failure of most of the soil. The depth and extent of the soil final failure surfaces were greater beneath the cables [Fig. 7(b)]. This may be due to the gradual increase in soil pressure along the height direction (Z-direction). Therefore, the fill soil above the cables exhibited less resistance, which led to the first cracking and appearance of failure in this soil area (Fig. 6). Furthermore, the soil above the cables failed when the pullout force was substantially large, and the pullout force was mainly resisted by the soil beneath the cables.

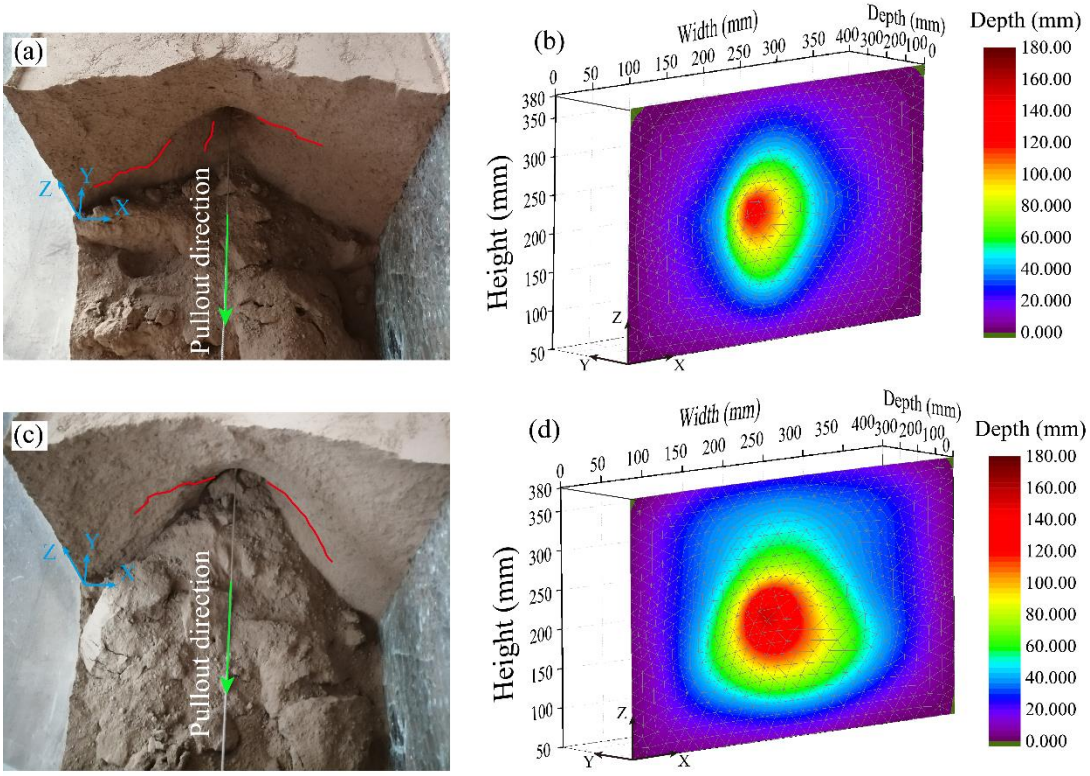

Fig. 7. Soil final failure surface under the pullout force of the single cable: (a) Photo of the soil final failure surface (D=7 mm); (b) Three-dimensional contour of the soil final failure surface (D=7 mm); (c) Photo of the soil final failure surface (D=10 mm); (d) Three-dimensional contour of the soil final failure surface (D=10 mm).

Results of the radial cable

Pullout performance of the radial cable

The curves (P-S curves) of the pullout force (P) versus displacement (S) of all radial cables (D=7 and D=10 mm) are plotted in Fig. 8. The P-S curves for all working conditions are basically identical to those for the single cables with anchor plates (Fig. 5). Additionally, the curves in Fig. 8 also exhibit a "saddle shape" and can be divided into four stages. The P-S curve of the radial cable (D=7

mm and β=15°) was used as an example for a detailed analysis [Fig. 8(a)]. As shown in Fig. 8(a), the first stage (S-1) was the elastic stage (OA section), and the pullout force linearly increased with the displacement owing to the minor pullout force acting on the radial cable during this stage. The second stage (S-2) was the elastic-plastic stage (AB section), when the pullout force reached 95.18 % of the P_u (Point B, which is the second inflection point in Fig. 8(a)). As can be seen, the first inflection point (Point A) of the P-S curve appeared at this moment. Simultaneously, the gradient of the curve became smaller, and the curve no longer linearly increased with the displacement. The third stage (S-3) was the softening stage (BC section), during which the pullout force gradually decreased with the displacement owing to the further expansion of the plastic zone of the soil around the radial cable under the effect of the pullout force. Furthermore, the friction between the radial cable and fill soil gradually reduced, and the soil surrounding the radial cable gradually failed. Consequently, the pullout force was mainly resisted by the anchor plate at this stage. The fourth stage (S-4) was the failure stage (CE section), which originated from the third inflection point (Point C) of the P-S curve. During this stage, the surrounding soil completely lost its bearing capacity (Fig. 8(a)). Meanwhile, the pullout force decreased rapidly with a large negative gradient, and the radial cable finally lost its pullout bearing capacity.

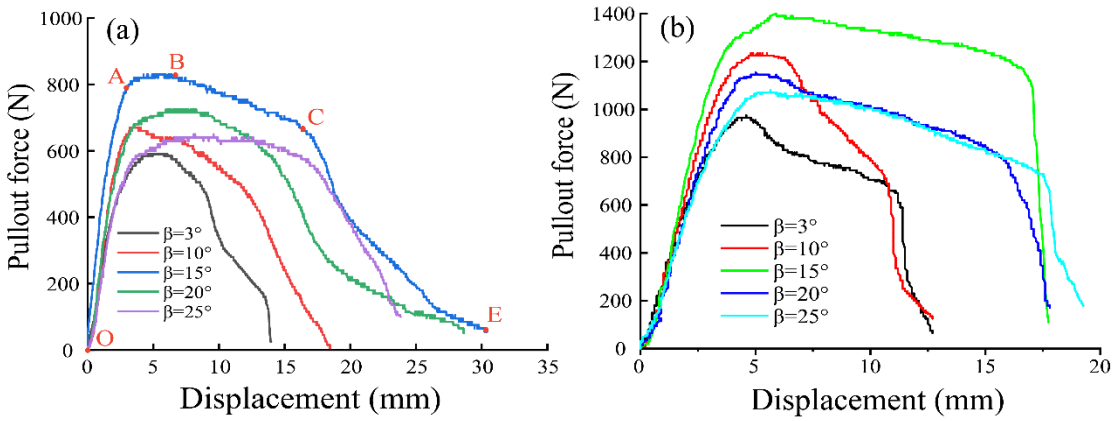

Fig. 8. Curves of the pullout force versus displacement of the radial cable: (a) D =7 mm; (b) D = 10

mm.

The P_u of the radial cable first increased with the increase in β, and their maximum values appeared at β=15°. However, for β>15°, the P_u gradually decreased with β [Fig. 8 and Fig. 9(a)]. Therefore, β=15° is the optimum radial inclined angle for the radial cable with anchor plates. The soil areas that resist the pullout force of sub-cables overlapped each other when β (<15°) was too small. Consequently, the soil areas that resist the pullout force of the radial cable decreased correspondingly resulting in a lower pullout capacity of the radial cable. Whereas, when β (>15°) was too large, the effective bearing section area of the anchor plates along the pullout direction was less. However, the soil areas that resist the pullout force of each sub-cable and radial cable gradually become independent of each other and decrease, respectively. Simultaneously, the depth of the sub-cables in the soil and effective pullout length of the branch sub-cables decreased for large values of β (>15°), which lead to a smaller pullout capacity of the radial cable. For β=15°, the resultant force of the cable side friction and anchor plate end resistance and side friction were optimal, and the soil around the radial cable used for resisting was fully mobilized. Therefore, the P_u was maximum under this working conditions.

As shown in Fig. 8, the third and fourth stages of the P-S curves are of crucial importance as they represent the deformation and damage characteristics of the radial cables after the pullout force reaches their P_u. Therefore, the magnitude of the displacements in these two stages are closely relevant for the prediction and warning of a potential failure of the fill soil, as the greater the displacement in these two stages, the longer the failure process. Thus, this long failure process can provide sufficient response time for early warning of geohazards and preventing sudden disasters

caused by sudden fill slope failures. The displacements during S-3 of the radial cables are shown in the Fig. 9(b). The displacement during S-3 was large and even greater for D=10 mm and the same β (β=15–25°). This indicates that the failure process of the radial cable was longer for β=15–25° and the safety of the radial cable improved at this moment.

The displacement corresponding to the $P \geq 80\% P_u$ (P is the pullout force) during S-3 of the P-S curves in Fig. 8 is called the "load holding stage", and the radial cable is still considered to exhibit a great pullout capacity. The ratio of the displacement during the load holding stage to the displacement from S-1 to S-3 is defined as the load holding ratio γ, which is calculated as follows:

$$\gamma = d_3/d, \quad (1)$$

where d_3 is the displacement during the load holding stage; d is the total displacement of the radial cables from S-1 to S-3.

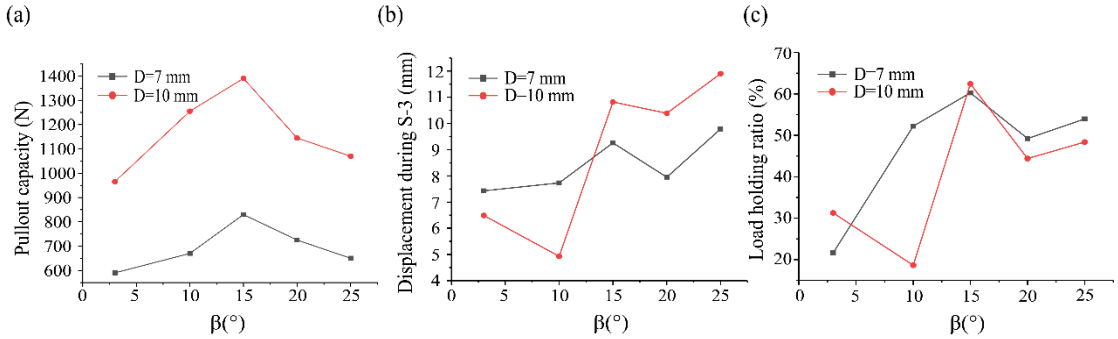

Fig. 9. (a) Curves of the ultimate pullout bearing capacity versus the radial inclined angle; (b) Curves of the displacement during S-3 versus the radial inclined angle; (c) Curves of the load holding ratio versus the radial inclined angle.

The variation of γ under different working conditions is shown in Fig. 9(c). For β=15°, the maximum value of γ was reached, and the maximum values of γ for different values of D were almost identical [Fig. 9(c)]. This indicated that the radial cable exhibited an excellent pullout bearing capacity and an outstanding load holding performance at β=15°. Consequently, although the radial

cables with D=10 mm failed suddenly during S-4, they still exhibited greater pullout capacity, safety, and γ [Fig. 8, Fig. 9(a), and Fig. 9(c)]. Therefore, anchor plate cross-section area should be designed as large as possible in practical engineering.

Failure process of the fill soil

The soil failure process of the radial cable (D=7 mm and β=15°) is described in detail as the failure processes of the radial cables are similar under all working conditions (Fig. 10). As shown in Fig. 10, the red lines, yellow areas, and green arrows represent the cracks, next potential failure area of the soil, and direction of the pullout force, respectively. The free surface of the soil was relatively smooth before loading, with only initial defects created during the filling of the soil [Fig. 10(a)]. During S-1 (OA section) [Fig. 10(i)], the soil was continuously compacted, and the pullout force on the radial cable was gradually increased. Subsequently, a micro-crack first appeared on the free surface of the fill soil at the upper and right of the radial cable. The micro-crack rapidly expanded above the cable [Fig. 10(b)], and then the soil below the pulling crack appeared significantly uplifted, simultaneously. After entering into S-2 (AB section) [Fig. 10(i)], the crack, as shown in Fig. 10(b), extended along the edge of its potential failure area, and an area on the free surface collapsed [Fig. 10(c)]. Subsequently, the crack on the right side of the radial cable also extended along the edge of the potential failure area [Fig. 10(c)], causing the collapse of the free surface at the right side of the radial cable [Fig. 10(d)]. Consequently, the collapse on the free surface on the left and right sides of the cable were temporally different, and the soil shear expansion phenomenon was apparent.

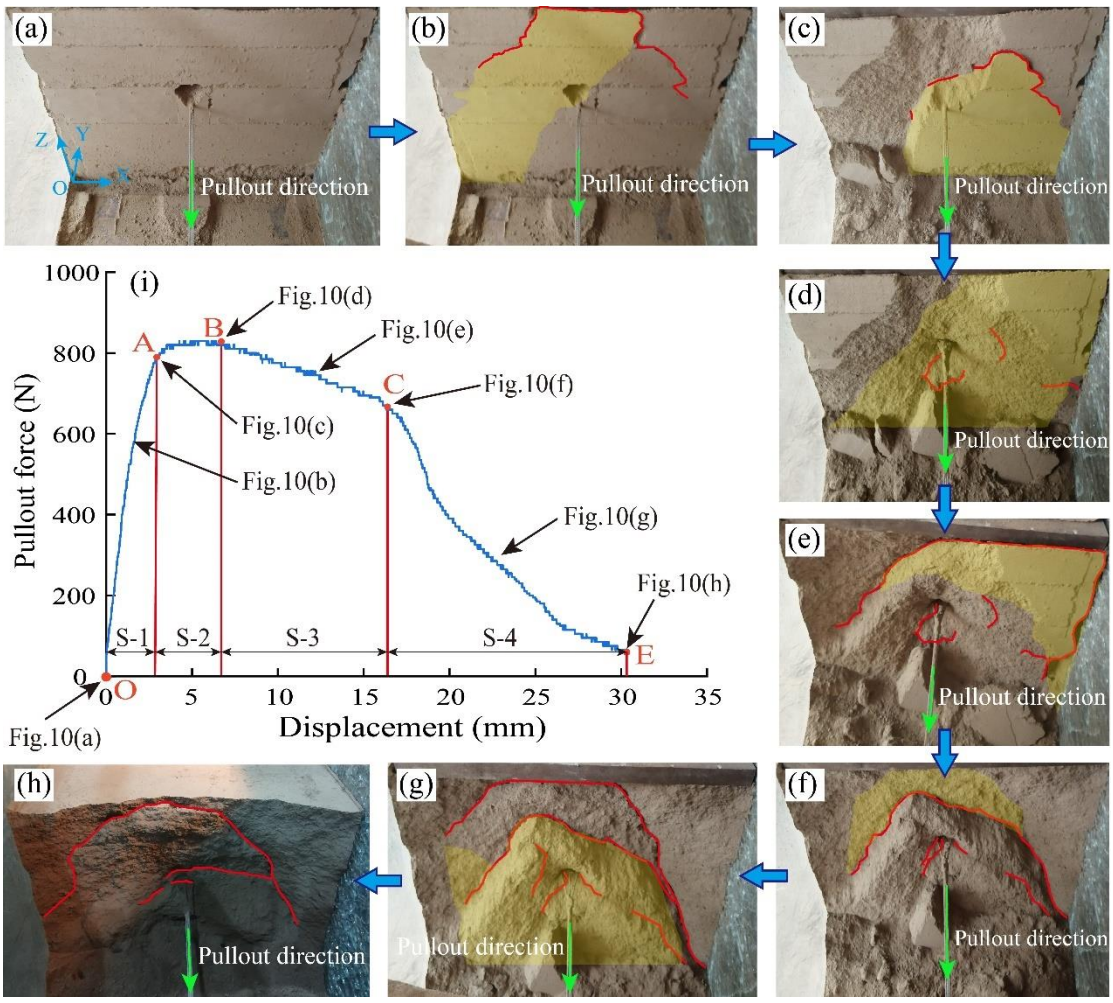

Fig. 10. (a)-(h) Photos of the soil failure process under the pullout force of radial cable with D=7 mm; (i) Pullout force versus displacement of the radial cable with D=7 mm.

When the P_u of the radial cable was reached, the free surface did not completely fail [Fig. 10(d)], indicating that the free surface still exhibited some bearing capacity. During S-3 (BC section), new tension cracks appeared in the fill soil, and their distribution range extended from the left and right sides of the radial cable to the right edge of the fill soil [Fig. 10(e)]. Simultaneously, the soil at the upper and right side of the radial cable stripped the original soil. Therefore, the initial free surface of the fill soil was completely failed, and then the soil failure range continued to develop along depth direction (Y-direction) [Fig. 10(e)]. During S-4 (CE section), the failed free surface at the right side of the radial cable completely collapsed [Fig. 10(f)], and the complete pullout force was

provided by the internal part of the fill soil. New and wide cracks at the upper part of the new free surface were observed with a further increase in the pullout force [Fig. 10 (f)–Fig. 10(g)]. When the radial cable was completely pulled out, the surrounding soil of the radial cable collapsed, and the failure depth of this area increased in the Y-direction [Fig. 10(h)]. Moreover, the soil final failure surface was observed to exhibit a "conical" pattern. Therefore, the depth (Y-direction) of soil failure was deeper near the radial cable and then gradually decreased away from it, and the symmetry of the soil final failure surface was observed [Fig. 10(h)]. In conclusion, the soil failure surrounding the radial cable along the depth direction (Y-direction) during the pullout force was a progressive process. The depth (Y-direction) of soil failure gradually increased, and the soil final failure surface showed a symmetrical "conical" pattern with an increase in the pullout force.

Final failure surface of the fill soil

The soil final failure surfaces of the radial cables and their three-dimensional contours under all working conditions are shown in Fig. 11 and Fig. 12. The initial free surfaces of the fill soil were all collapsed, and the soil final failure surfaces basically exhibited a "conical" pattern. Therefore, the failure depth (Y-direction) near the radial cable was the deepest, and then it gradually decreased along the direction away from the radial cable. At β=3°, the failure depth was deep and concentrated near the radial cable with a large gradient in depth [Fig. 11(a) and Fig. 12(a)]. This indicated that when β was minor, the soil final failure surface was similar to that of the single cable [Fig. 7, Fig. 11(a), and Fig. 12(a)]. The maximum failure depth and variation range of the failure depth continuously decreased with the β (β=3–15°). However, the failure area of the final failure surface decreased for β=15–25°, indicating that the fill soil, which resists the pullout force, was accordingly

reduced [Fig. 11(c)–Fig. 11(e) and Fig. 12(c)–Fig. 12(e)]. Consequently, the P_u of the radial cable decreased for β=15–25°.

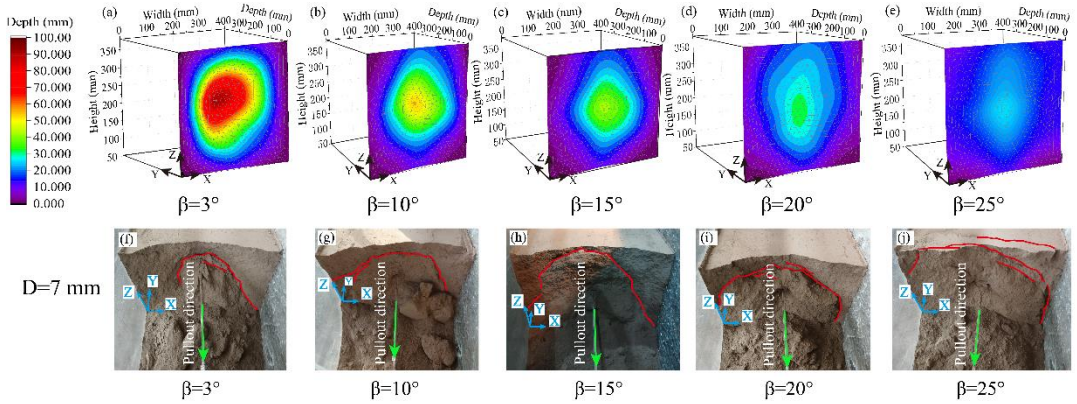

Fig. 11. Soil final failure surface under the pullout force of the radial cable with D=7 mm: (a)-(e) Three-dimensional contour of the soil final failure surface; (f)-(i) Photos of the soil final failure surface.

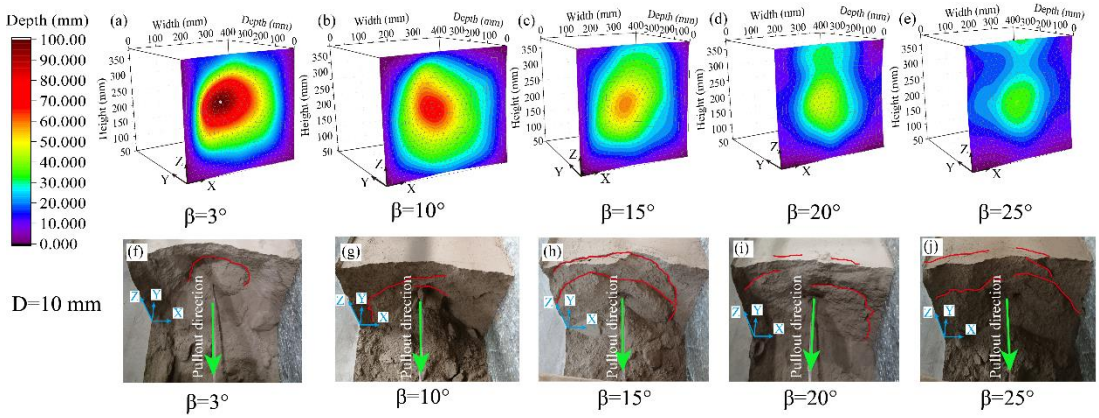

Fig. 12. Soil final failure surface under the pullout force of the radial cable with D=10 mm: (a)-(e) Three-dimensional contour of the soil final failure surface; (f)-(i) Photos of the soil final failure surface.

For identical values of β, the failure depth and range of the final failure surface of the radial cable with D=10 mm were significantly greater than those of the radial cable with D=7 mm [Fig. 11 and Fig. 12]. The increase in D expands the resistant range of the fill soil near the end of the sub-cables, and the radial cable resists a greater pullout force. Therefore, the P_u of the radial cable

significantly increased with the increase in D [Fig. 9(a)]. As shown in Fig. 11 and Fig. 12, the number and distribution extent of the cracks were more concentrated when β was minor. For instance, for β= 3°, only one main and obvious tension crack on the failure surface was observed [Fig. 11(f) and Fig. 12(f)]. The length of the main cracks, and number and distribution extent of the crack in the soil final failure surface gradually increased with the β (Fig. 11 and Fig. 12). For β= 25°, several tensile cracks with different lengths in the soil final failure surface were observed. Additionally, for β=20 or 25°, the distribution area of tensile cracks extended to the upper surface of the fill soil [Fig. 11(i)–Fig. 11(j) and Fig. 12(i)–Fig. 12(j)].

Comparative analysis between the single cable and the radial cable

The single cable and radial cable (β=15°) with D= 7 mm were selected for comparison. The P_u, displacement during S-3 (softening stage), and maximum failure depth of the final failure surface are shown in Fig. 13. The P_u of the radial cable was 4.15 times that of the single cable. This indicated that the greater pullout capacity provided by the radial cable effectively decreased the horizontal displacement of the fill soil, and then the stability of the fill-bedrock interface significantly improved. Furthermore, the displacement during S-3 of the radial cable was 2.17 times that of the single cable. Therefore, the pullout failure process of the radial cable was longer than that of the single cable. This indicated availability of more time for early warning about the slope failure and effective avoidance of property damage and casualties owing to the application of the radial cable. In short, the pullout performance of the radial cable significantly improved compared with that of the single cable.

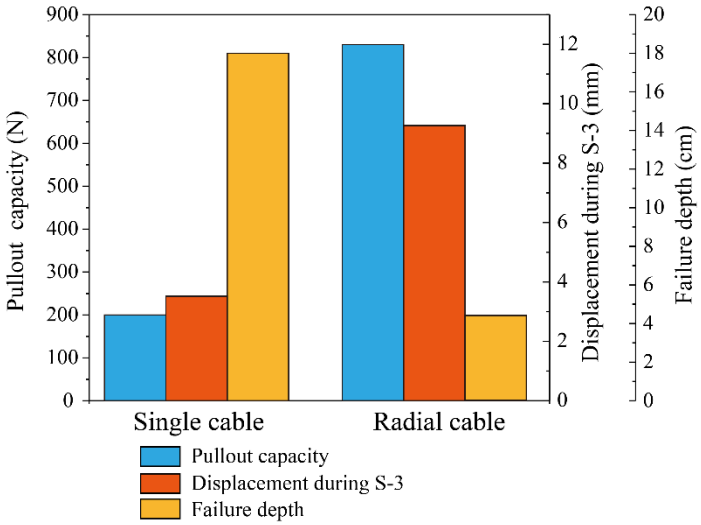

Fig. 13. Comparison between the single and the radial cable (β= 15°) with D=7 mm.

The maximum failure depth of the single cable was 2.63 times that of the radial cable (Fig. 13), and the gradient of the soil failure depth surrounding the single cable was greater [Fig. 7(a)–Fig. 7(b), Fig. 11(c), and Fig. 11(h)] indicating that the failure of the fill soil surrounding the single cable was concentrated near it. The soil failure range of the single cable was less than that of the radial cable [Fig. 7(a)–Fig. 7(b), Fig. 11(c), and Fig. 11(h)]. Therefore, the radial cable enables a larger volume of the fill soil to resist the pullout force, which increases its pullout capacity.

Application example

Engineering example and numerical model

A high fill project of an airport located in the mountainous area of Southwest China was used as an application example in this study [Fig. 14(a)]. Near the beginning of the third runway, the fill project was divided into two parts by a highway bridge [Fig. 14(b)–Fig. 14(c)]. Thus, the fill project could not be filled at once. Simultaneously, the expressway was not demolished on time owing to the coordination problems of all parties, resulting in a serious lag in the fill construction progress.

To minimize the negative impact of the expressway on the project and ensure the completion of the fill work on schedule, the fill works were undertaken on the inner and outer sides of the expressway bridge before the demolition of the bridge. The outer side was first filled near the bridge deck up to an elevation of 330 m a.s.l. [Fig. 14(c)]. The specific fill scheme is shown in Fig. 14(c). The areas of "1-fill" were the first to be filled, followed by the area of "2-fill." Finally, the area of "3-fill" was filled after the highway bridge was completely demolished. Bench excavation of the bedrock slope, composed of sandstones (denoted by the thick purple line in Fig. 14(c)), could not be carried out as the highway was still operational, and thus the slope inclination was steep (about 86°). The slope was approximately 20–40 m high and 100 m wide [Fig. 14(b)]. Consequently, high tensile stresses were expected at the steep fill-bedrock interface. These tensile stresses would generate tension cracks at the rear edge of the fill soil along the interface. Therefore, since the tension crack restraint capacity of the steep interface to the fill body was weak, the landslide of the fill soil could be easily triggered. Therefore, the radial cable system was recommended for reinforcing the fill soil under this working condition to ensure the stability of the steep fill-bedrock interface.

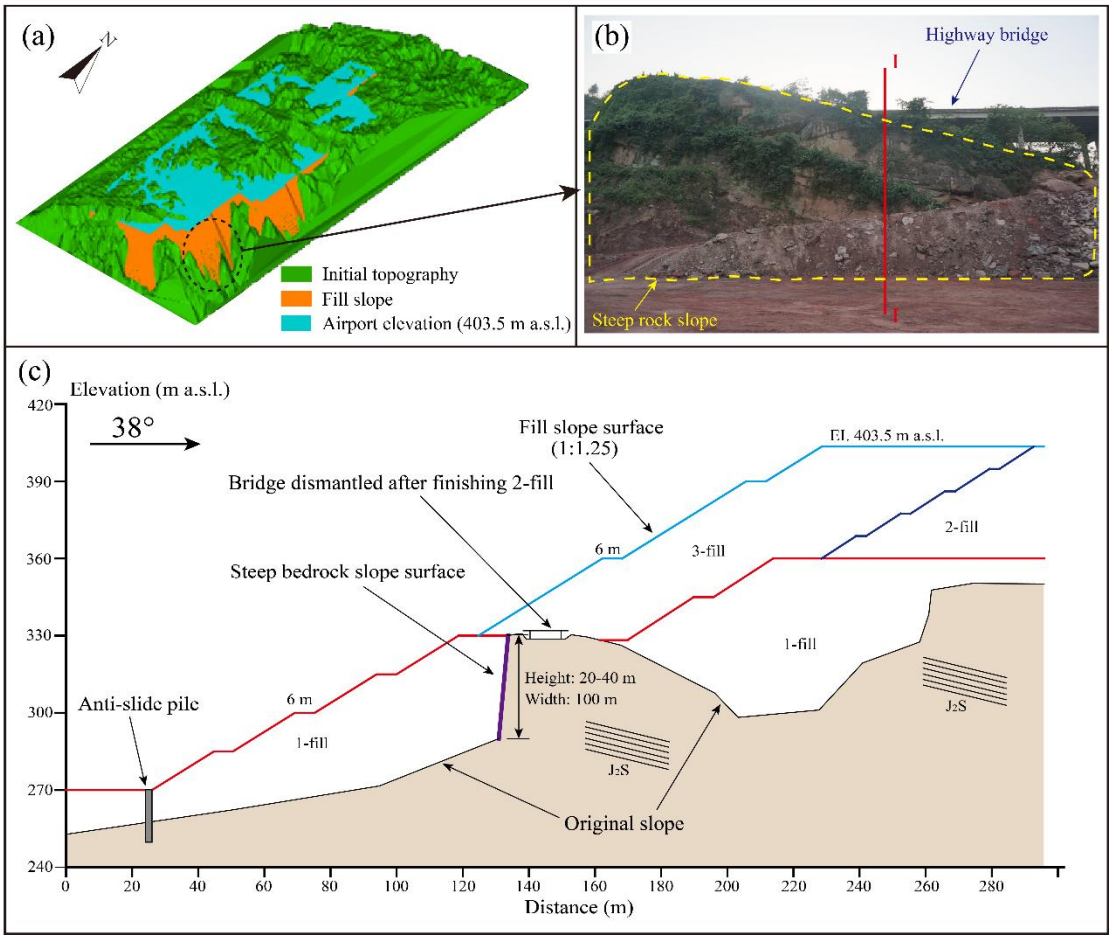

Fig. 14. Introduction of the high-fill project: (a) Digital elevation model of the high fill performed in the expansion project of the Chongqing Jiangbei International Airport (China); (b) Photo of the steep rock slope; (C) Geological profile and fill scheme of the steep rock slope (modified from Huang et al. 2019). Note: J_2S represents the bedding of the rock mass.

To assess the reinforcement effect of the radial cable system in this actual project, numerical models were established by ABAQUS 3D finite element software for three scenarios: a) unreinforced fill slope; b) fill slope reinforced by the conventional cables; and c) fill slope reinforced by the radial cables. To improve the efficiency of the calculation, the original profile, as shown in Fig. 14(c), was simplified, and the main features were retained, as shown in Fig. 15. The length (X-direction), height (Z-direction) and wide (Y-direction) of the slope model were 110, 62 and 30 m, respectively. The angles of slope of the bedrock at the interface were not fixed, with 9° in the front

side, 30° in the middle, and 86° in the upper part. A stepped design was adopted for the fill slope. The slope of each step was 1:1.25, with a 6 m terrace at 10 m intervals along the height direction (Z-direction); the height of the steep bedrock slope surface was 20 m [Fig. 15(d)]. Four rows of the cables (labelled as rows 1 to 4 from top to bottom) were arranged at the distances of 3, 8, 13 and 18 m from the top of the fill slope. Four cables were arranged in each row with an out-of-plane spacing of 6 m between adjacent cables in the same row. Furthermore, the adjacent rows of cables were arranged in a staggered pattern [Fig. 15(a)–Fig. 15(b)]. Shear keys with the circular cross-section were arranged directly above the cables for resisting shear stress at the interface and preventing shear damage of the cables. The length of the shear keys embedded in the bedrock was 2.0 m, and the length buried in the fill soil was 2.5 m. According to the results of the pullout test, the angle of the radial cables was set at 15° for ensuring the maximum pullout capacity of the single cable. The lengths of the anchorage section of the radial cable embedded in the bedrock and each sub-cable buried in the fill soil were 5 and 10 m, respectively. Therefore, the adopted radial cable system consisted of radial cables, shear keys, and anchor plates. The "U" shaped rigid rods, horizontal inclined angle between the cables in the anchorage section, and cables in the reinforcement section "α" were not considered (Fig. 2). The anchor plates were evenly installed on each sub-cable, and the distance between each anchor plate installed on the same sub-cable was 2 m (Fig. 15).

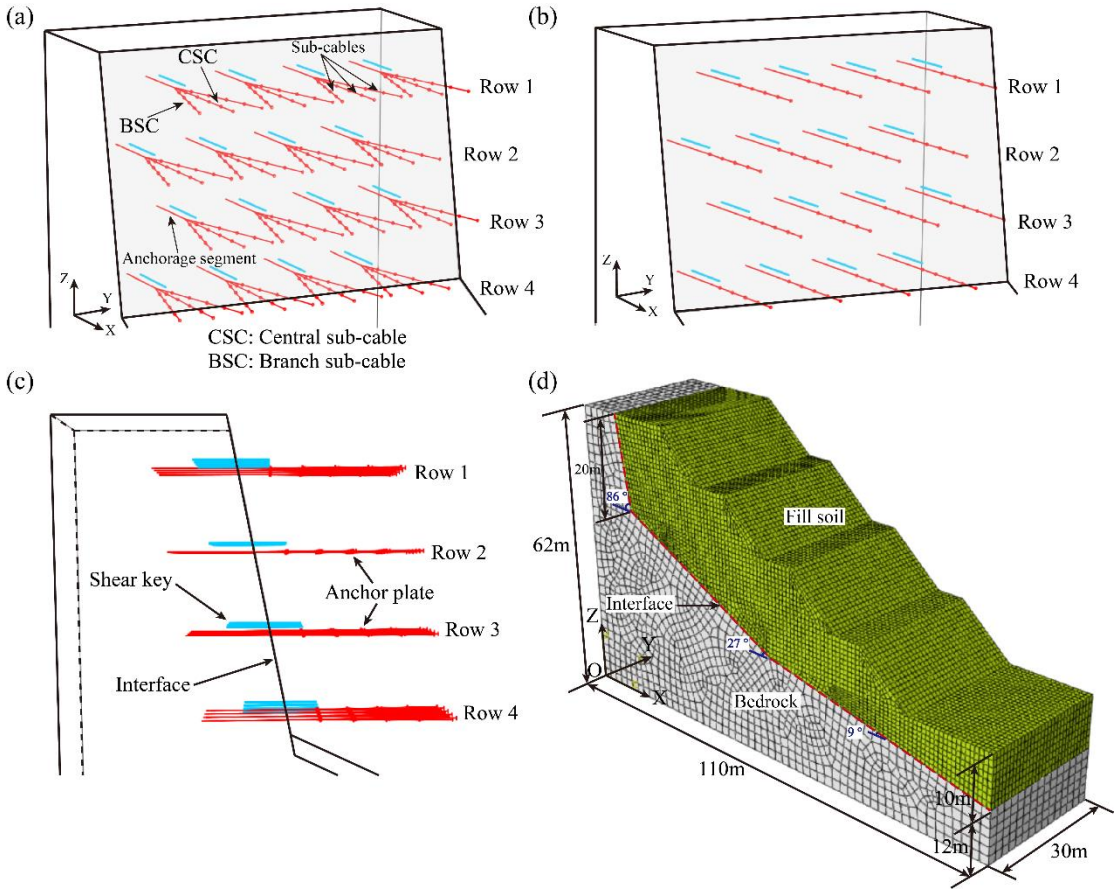

Fig. 15. Three-dimensional numerical model of the airport high-fill project: (a) Details of the radial cable system; (b) Details of the conventional cable system; (c) Side view of the radial cable system; (d) Numerical model.

A complete elastic model was adopted for the cables, anchor plates, and shear keys, and an elastoplastic Mohr-Coulomb model with non-associated flow rule was adopted for the fill soil and bedrock. The specific material parameters of the numerical model are listed in Table 3. The general contact algorithm was adopted for modelling the interface between the fill soil and bedrock. “Hard” contact conditions were employed for the normal behaviors; “Penalty function method” with Coulomb frictional law was used for the tangential behaviors. The cables, anchor plates, and shear keys were embedded in the fill soil and bedrock in the built-in areas. The bottom and side surfaces of the slope model were constrained to displacement in all three and normal directions, respectively; and the top surface of the slope model was free. After the completion of the fill work of the steep

slope, a uniform load of 108 kPa (equivalent to 4.8 m high fill) was applied to the top surface of the fill soil to simulate the gravity load of the subsequent fill ("3-fill" in Fig. 14(c)) to be placed above it. The cables and anchor plates were meshed by two-node three-dimensional truss elements (T3D2) with an average mesh size of 0.25 m; the shear keys were meshed by two-node spatial linear beam elements (B31) with an average grid mesh of 0.25 m. The bedrock and fill soil were meshed by three-dimensional eight-node linear hexahedral elements (C3D8) with an average mesh size of approximately 1 and 3 m for the fill soil and bedrock, respectively. Notably, the fill slope reinforced by conventional cables and radial cables differed only in the type of the cable system to achieve a better comparative analysis [Fig. 15(a)–Fig. 15(b)].

Table 3. Properties of the materials.

Material	Density (kg/m^3)	Elastic modulus (MPa)	Friction angle (°)	Cohesion (KPa)	Poisson's ratio	Cross-section (cm^2)
Fill (Silty clay)	2280	200.40	29.40	8.24	0.30	-
Rock (Sandstone)	2650	200.40×10^4	45	2×10^4	0.30	-
Anchor plate (Steel plate)	-	2×10^5	-	-	0.25	300
Cable (Steel rope)	-	1×10^8	-	-	0.25	7.00 (2.30 for sub-cables)
Shear key (Steel pipe and concrete)	-	8×10^4	-	-	0.25	78.50

Note: The parameters of the materials in Table 3 were referred from the published work (Huang et al. 2019) and the investigation report of the high fill work of the Chongqing Jiangbei International Airport (China).

Deformation of the fill slope

The slope horizontal displacement contours for the three scenarios described in the previous section are shown in Fig. 16, where Fig. 16(a)–(c) and Fig. 16(d)–(f) show the slope profiles with Y=15 m and Z=49 m, respectively. An obvious tension crack appeared at the interface of the unreinforced fill slope, exhibiting width of 2.30–3.30 mm and a maximum horizontal displacement of 5.73 mm [Fig. 16(a)]. Meanwhile, when the horizontal displacement was large (5.24–5.73 mm, Fig. 16(a)), its distribution range was wide in the fill soil, indicating seriousness of the failure of the unreinforced fill slope.

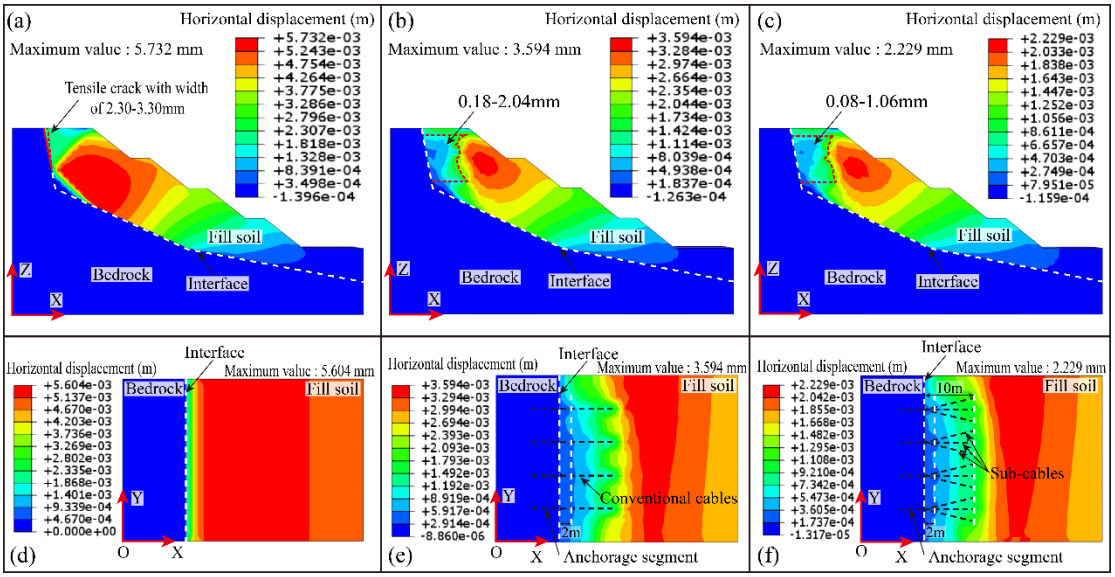

Fig. 16. Contour of the horizontal displacement of the fill slope: (a) Unreinforced (profile of Y=15 m); (b) Reinforced by the conventional cable (profile of Y=15 m); (c) Reinforced by the radial cable (profile of Y=15 m); (d) Unreinforced (profile of Z=49 m); (e) Reinforced by the conventional cable (profile of Z=49 m); (f) Reinforced by the radial cable (profile of Z=49 m).

Conversely, when the fill slope was reinforced by conventional cables [Fig. 16(b)], its maximum horizontal displacement was 3.594 mm (37.30% lower than that of the unreinforced fill slope), and the horizontal displacement of the fill slope was significantly reduced within the area of influence

of the cable reinforcement (i.e., within the red dashed line in Fig. 16(b), the horizontal displacement was 0.18–2.04 mm). Additionally, the horizontal displacement distribution of the fill slope was more uniform, and no concentrated failure areas existed.

Finally, when the fill slope was reinforced by radial cables [Fig. 16(c)], the maximum horizontal displacement was 2.23 mm (61.11% lower than that of the unreinforced fill slope and 37.98% lower than that of the fill slope reinforced by conventional cables). Moreover, the horizontal displacements of the slope within the area of influence of the radial cable reinforcement (i.e., within the red dashed line in Fig. 16(c)) reduced from 48.07 to 55.55% compared with the area of influence of the conventional cable reinforcement [Fig. 16(b)]. This indicated that the reinforcement effect of the radial cables was obviously better than that of the conventional cables.

The slope horizontal displacement contours of three scenarios with Z=49 m profile are shown in Fig. 16(d)–Fig. 16(f). For the unreinforced fill slope, the horizontal displacement first increased and then slightly decreased along the direction away from the interface, attaining a maximum horizontal displacement of 5.60 mm [Fig. 16(d)]. For the fill slope reinforced by conventional cables [Fig. 16(e)], the horizontal displacement near the cables significantly reduced, and an obvious soil arching effect between cables was observed. This indicated that the horizontal displacement in the area reinforced by conventional cables was different. Thus, the constraint of conventional cables on horizontal displacement was uneven. For fill slope reinforced by radial cables [Fig. 16(f)], the horizontal displacement within the radial cable reinforcement area was more evenly distributed. This indicated that the radial cables can reinforce a larger area of the fill soil and effectively control the horizontal displacement of the fill slope. At 2 m from the interface, the horizontal displacements were approximately 0.59 and 0.36 mm, as shown in Fig. 16(e) and Fig. 16(f), respectively; at 10 m

from the interface, the horizontal displacements were approximately 2.09 and 1.29 mm, as shown in Fig. 16(e) and Fig. 16(f), respectively. Consequently, the branched sub-cables can efficiently grasp fill soil and increase cohesion between the fill soil and bedrock (Huang et al. 2019).

The fill slope horizontal displacement near the interface of three scenarios are shown in Fig. 17. The maximum values of the horizontal displacements appeared at the ground surface of the fill soil, and then the horizontal displacements gradually decreased with depth [Fig. 17(a)]. Consequently, these results show that the horizontal displacement of fill slope reinforced by conventional or radial cables was significantly lower than that of the unreinforced fill slope. Furthermore, the horizontal displacement of the fill slope reinforced by radial cables was less than that reinforced by conventional cables. As shown in Fig. 17(a), an inflection point of the horizontal-depth curve of the unreinforced fill slope appeared near the depth of 13 m, indicating that the horizontal displacement was relatively concentrated at lower depths. Conversely, no obvious inflection points in the other curves were observed [Fig. 17(a)], indicating the horizontal displacements of the fill slopes reinforced by cables to be more uniform.

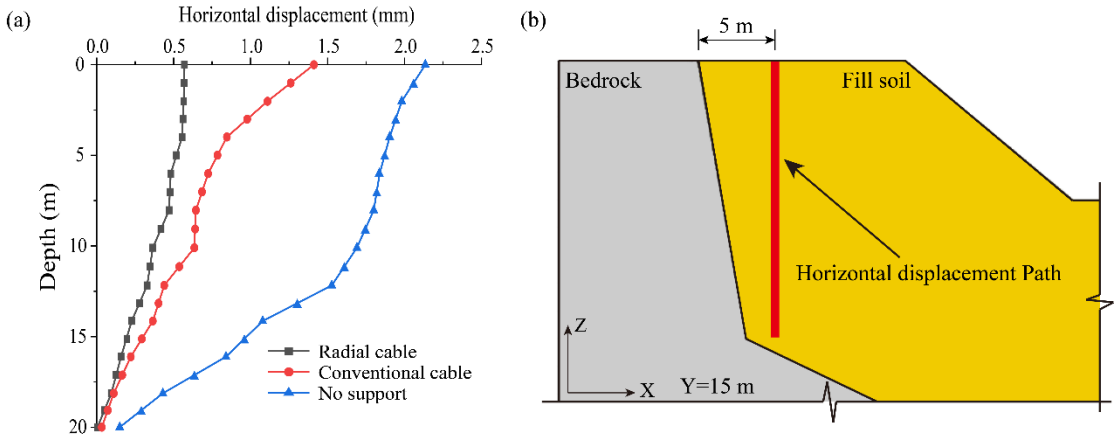

Fig. 17. Horizontal displacements of the fill near the interface: (a) Curves of the horizontal displacement versus depth; (b) Horizontal displacement path.

Axial force of the cables

The average axial forces of the anchorage segment of all rows are shown in Fig. 18. The average axial force of the radial cables decreased essentially linearly with depth [Fig. 18(a)], and the average axial force of the conventional cables increased first from Rows 1 to 3 and then gradually from Rows 3 to 4 [Fig. 18(b)]. This indicated that the reinforcement performance of the radial cables was more stable and effective, while the reinforcement effect of conventional cables in the Row 1 was significantly reduced.

The axial forces at five representative junctions of each sub-cable to plot the axial force distribution curves of the central and branch sub-cables are depicted in Fig. 19. The axial forces of the sub-cables decreased away from the interface, and the most significant difference between the axial forces of the sub-cables was observed at approximately 2–4 m (ID from 1 to 2) from the interface. Additionally, the axial forces of the sub-cables decreased with the depth when their ID were identical. The decay rates of the axial force of the branch anchor ropes were slow at approximately 2–4 m (ID from 1 to 2) from the interface; however, they significantly increased at approximately 8–10 m (ID from 4 to 5) from the interface. In the same row, the axial force of the central sub-cable was greater by approximately 74–189 kN than that of the branch sub-cables [Fig. 19].

As can be seen from Fig. 18 and Fig. 19, the axial forces of the radial cables located in the shallow buried depth were greater than that located deeper in the buried depth. Consequently, the diameter and elastic modulus of the radial cable in shallow buried depth should be appropriately increased to further improve the reinforcement effect when designing them. For instance, the spacings of radial cables in the same row and of each row should be reduced in this area.

Furthermore, the diameter and length of sub-cables and the cross-sectional area of anchor plates should be increased in this area. Additionally, in one radial cable, the diameter, elastic modulus, and anchor plate cross-sectional area of the central sub-cable should also be appropriately increased compared with the branch sub-cable.

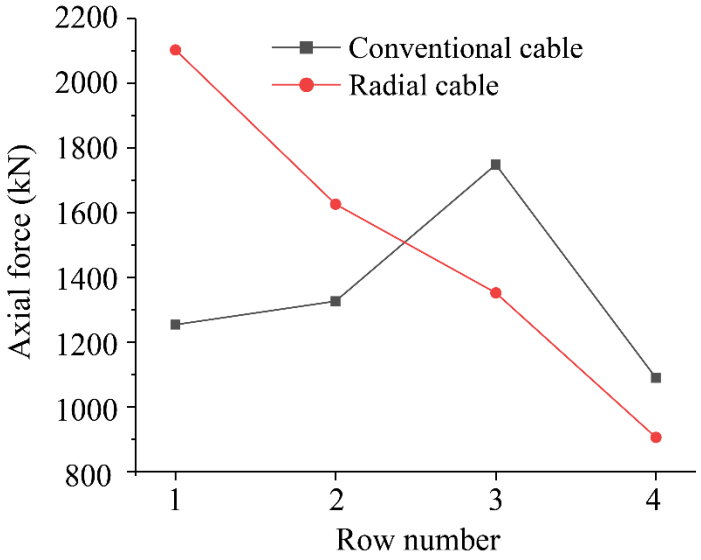

Fig. 18. Curves of the average axial force of the anchorage segment for each row.

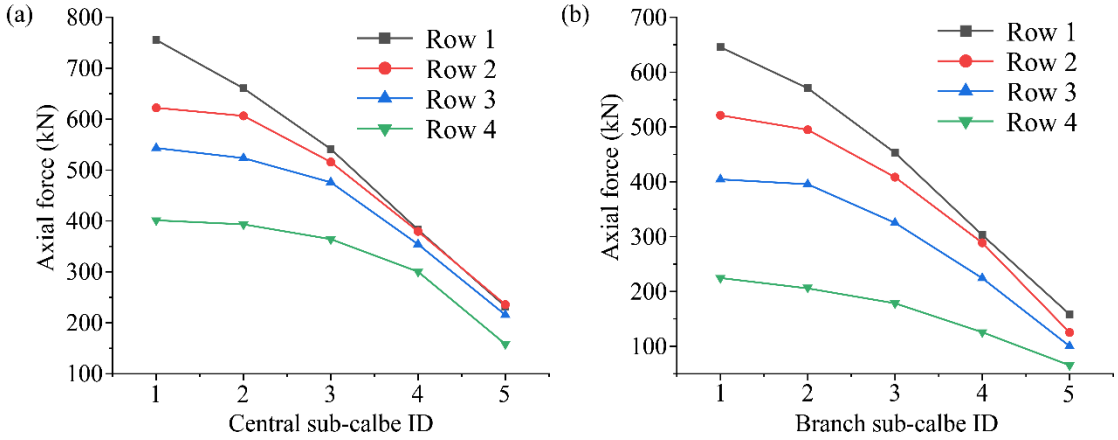

Fig. 19. Axial force of sub-cables: (a) Central sub-cables; (b) Branch sub-cables. Note that the axial force represented in this figure corresponds to the third cable (from left to right) in every row (Fig. 15a-b).

Discussion

Failure mechanism of the single and radial cables with the anchor plate

The failure mechanisms of the single cable (with D=7 mm) and radial cable (with D=7 mm and β=15°) are explained by Fig. 20(a) and (b). The final failure surfaces of the single and radial cables shown a “conical” distribution near cables (Fig. 7, Fig. 11, and Fig. 12), which was similar to the pullout surface of anchor plates (Meyerhof 1968; Dyson and Rognon 2014; Evans and Zhang 2019). Accordingly, based on the pullout failure surface of anchor plates (Meyerhof 1968; Dyson and Rognon 2014; Evans and Zhang 2019) and the final failure surface of the fill soil (Fig. 7, Fig.11, and Fig. 12), the displacement area and failure surface of the single and radial cables were obtained [Fig. 20(a) and (b)]. Besides, the distribution law of the displacement areas and failure surfaces of each sub-cable were obtained based on the single cable [Fig. 20(b)]. Thus, the failure mechanisms of the single and radial cables were the failure of the soil shear strength in displacement area. The displacement areas of each sub-cable overlapped each other under the branching effect of radial cable, and they formed a new displacement area [Fig. 20(b)]. This demonstrated that the volume of fill soil that mobilized to resist pullout force acting on the radial cable was significantly greater than that of the single cable (Fig. 20). Consequently, with the radial arrangement, the radial cable can mobilize larger region of fill soil to resist the pullout force, resulting in its considerably increased pullout capacity.

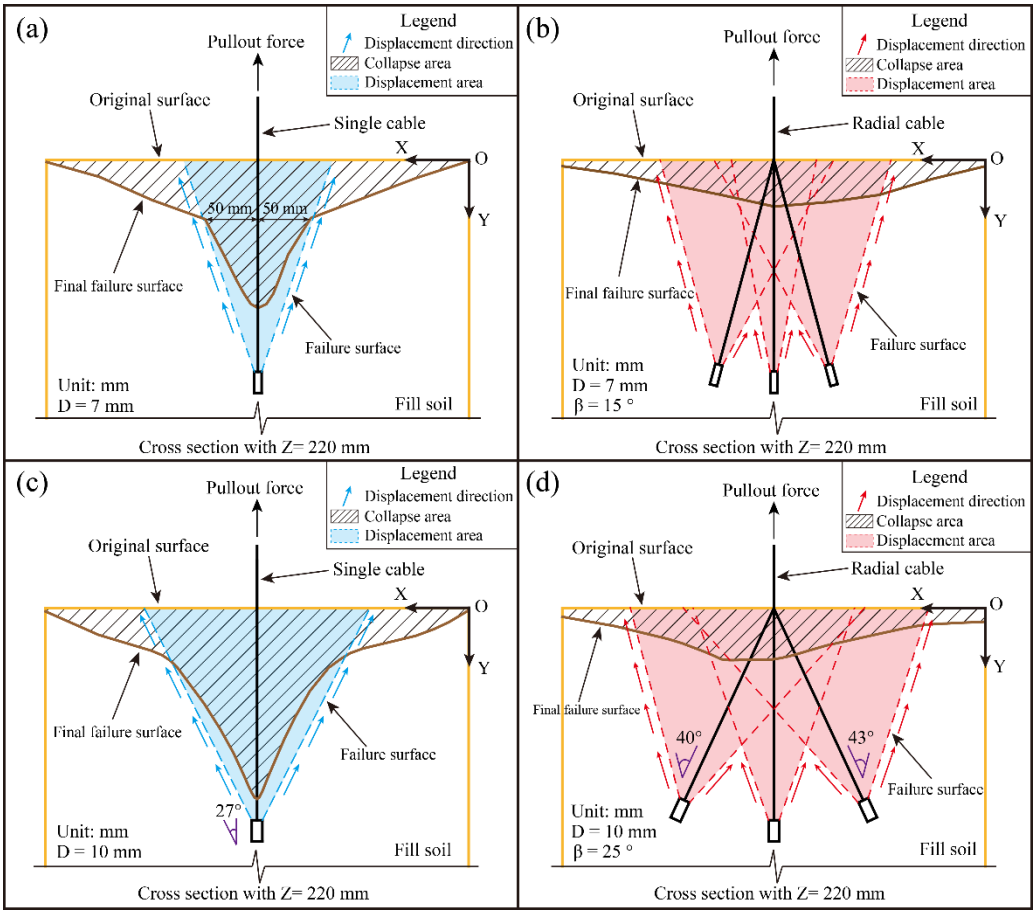

Fig. 20. Schematic of the soil failure pattern: (a) Single cable (D= 7 mm); (b) Radial cable (β= 15 ° and D= 7 mm); (c) Single cable (D=10 mm); (d) Radial cable (β= 25° and D= 10mm).

The horizontal pullout force was applied in the pullout test, and the original failure surface of the fill soil was a vertical free surface. Therefore, the heave of the fill soil on the failure surface was hardly observed during the pullout process. Meanwhile, the free surface easily collapsed owing to the effect of the horizontal pullout force and gravity (Fig. 7, Fig. 11, and Fig. 12). The maximum failure depth of the collapse area for the single cable was 140 mm, whereas it was only 44 mm for the radial cable [Fig. 20(a) and (b)]. Furthermore, the collapse area of the single cable concentrated on the surrounding of the single cable, and its depth significantly increased in the area within 50 mm from the single cable [Fig. 20(a)]. Inversely, the depth of failure of the collapsed area of the radial cable was more uniform than that of the single cable, and the volume of the collapsed area of

the radial cable was less than that of the single cable [Fig. 20(a)]. This indicated that the fill soil reinforced by the single cable could be failed more easily, and the failure hazard is greater compared with the fill soil reinforced by the radial cable. Notably, during the pullout process of the radial cable, the soil did not suddenly collapse in a small range as observed during the pullout process of the single cables, indicating that the radial cables have better pullout performance and safety.

Size effect of the pullout test

For D=10 mm, the single and radial cables both exhibited bigger soil failure areas (Fig. 7 and Fig. 12). Meanwhile, for D=10 mm and β=25°, the distance from the radial cable to the inwall of the model box was minimum. Therefore, the single cable with D=10 mm and radial cable with D=10 mm and β=25° were selected to explain the size effect. According to the methodology described above, their displacement areas and failure surfaces are shown in [Fig. 20(c) and (d)]. The inclination of failure surface of single cable was 27°, and the inclination of failure surface of sub-cables (near the inner wall sides of the model box) were 40 and 43°, indicating that the displacement area of the radial cable shown in Fig. 20(d) was conservative enough. Additionally, the displacement areas of the single cable and radial cable were both inside the fill soil compacted in the model box [Fig. 20(c) and (d)]. The failure depths of the soil located at the edge of the fill soil were minor (Fig. 7, Fig.11, Fig.12, and Fig. 20); and except for the failure area near the initial free surface, no visible cracks or failure were observed through the tempered glass on the fill soil side. Consequently, the size of the model box was big enough to test the pullout performance of the cables, and the influence of size effect could be accepted. However, the free surface of fill soil was characterized by overall spalling rather than local counterpart (Fig. 7, Fig. 11, and Fig. 12) as the free surface was vertical

and the free surface collapsed owing to the slight disturbance and action of the gravity. In the follow-up study, a bigger setup will be used for the pullout test of the radial cable to decrease the influence of the size effect to the maximum extent possible.

Conclusions

The radial cable system was proposed for effectively reinforcing steep fill-bedrock interfaces. The pullout performance, branching effect, and failure process of the radial cable were studied using a series of pullout tests. Additionally, the proposed radial cable system was applied to an actual project through a numerical simulation, and its reinforcement effect was verified. The main conclusions of this study are summarized as follows:

(1) The P_u of single cables with anchor plates is 40.56 and 179.72 % greater than single cables without anchor plates. Under identical working conditions, the P_u of the radial cables is 193.53–312.94 % (D=7 mm) and 141.25–247.50 % (D=10 mm) greater than that of the single cables (conventional cables). Furthermore, the failure displacement of the radial cables is greater for β>10°, indicating their significantly higher safety than that of the single cables. The P_u of the radial cables is remarkably affected by β, and it gradually increases when β is varied from 3 to 15° and gradually decreases for β >15°. Therefore, the optimum β is 15°, and the value of the P_u of the radial cable is maximum at this moment. Additionally, the P_u of the single cables increases by 57.93–87.31 % with an increase in D under the identical working condition.

(2) The soil failure process under all working conditions is a progressive failure. Therefore, the fine cracks first appear on the initial free surface of the fill soil and gradually expand and penetrate under the effect of the pullout force, resulting in the gradual collapse at the free surface of the fill

soil. Subsequently, the fill soil near the cables locally collapses, and the failure depth further increases. When the cables completely lose their pullout capacities, the soil final failure surface shows a symmetric "conical" pattern. Consequently, the soil final failure surface is deepest at the cables, and the failure depth gradually decreases along the direction away from the cables and pullout direction. As the D increases, the soil final failure surface depth deepens and the failure area enlarges. Besides, the failure depth and failure area gradually decrease for β=15–25°. The soil final failure surface depth of the single cable significantly increases near it, and its maximum failure depth is greater than that of the radial cables under the same working condition.

(3) In actual application, compared with the conventional cable system, the radial cable system can more effectively control the horizontal displacement of fill soil near the high steep fill-bedrock interface. Hence, the stability of the fill slope is improved, and the possibility of the landslide triggered by the separation between the fill soil and bedrock is reduced. The axial forces of the upper row of the radial cables are greater, and they decrease with buried depth. Moreover, the axial forces of the central sub-cables in one radial cable are greater by 74–189 kN than those of the branch sub-cables; and the axial forces of sub-cables decrease along the direction away from the interface.

In this study, the soil properties and overlying pressure were constant, and this is the limitation of our study. If the soil layer or overlying pressure are both changed, the shear strength and stress state of the fill soil, and the pullout capacity of the radial cable will also be affected. However, in the absence of substantial experimental or numerical evidence, we cannot determine the impact of various soil layers and overlying pressures on optimum angle of the radial cable. Consequently, in a subsequent study, the impact of various soil layers and overlying pressures on optimum angle of the radial cable will be explored.

Data Availability Statement

All data, models, or code that support the findings of this study are available from the corresponding author upon reasonable request.

Acknowledgments

This work is supported by the National Natural Science Foundation of China (41972297), Natural Science Foundation of Hebei Provincial Natural (D2021202002), Scientific research project from the Education Department of Hunan Province (21C0753), Changsha Municipal Natural Science Foundation (kq2202065), and Hunan Provincial Natural Science Foundation (2022JJ40521). The author Roberto Tomas is supported by the ESA-MOST China DRAGON-5 project (ref. 59339).

References

Abdi, M. R., and A. R. Zandieh. 2014. "Experimental and numerical analysis of large scale pull out tests conducted on clays reinforced with geogrids encapsulated with coarse material." *Geotext Geomembranes* 42 (5):494-504. doi: 10.1016/j.geotexmem.2014.07.008.

Alam, Md Jahid Iftekhar, S. R. Lo, and M. R. Karim. 2014. "Pull-out behaviour of steel grid soil reinforcement embedded in silty sand." *Comput Geotech* 56:216-26. doi: 10.1016/j.compgeo.2013.12.004.

Bhattacharya, Paramita, and Jyant Kumar. 2014. "Pullout capacity of inclined plate anchors embedded in sand." *Can Geotech J* 51 (11):1365-70. doi: 10.1139/cgj-2014-0114.

Bru, G., J. A. Fernandez-Merodo, J. C. Garcia-Davalillo, G. Herrera, and J. Fernandez. 2018. "Site scale modeling of slow-moving landslides, a 3D viscoplastic finite element modeling approach."

Landslides 15 (2):257-72. doi: 10.1007/s10346-017-0867-y.

Cao, G. X., E. X. Song, and M. Xu. 2011. "Simplified calculation methods of post-construction settlement of high-fill foundation in mountain airport." *Rock Soil Mech* 32:1-5+26. doi: 10.16285/j.rsm.2011.s1.081.

Carey, J. M., B. Cosgrove, K. Norton, C. I. Massey, D. N. Petley, and B. Lyndsell. 2021. "Debris flow-slide initiation mechanisms in fill slopes, Wellington, New Zealand." *Landslides* 18 (6):2061-72. doi: 10.1007/s10346-021-01624-6.

Cen, Duofeng, Da Huang, and Feng Ren. 2017. "Shear deformation and strength of the interphase between the soil-rock mixture and the benched bedrock slope surface." *Acta Geotech* 12 (2):391-413. doi: 10.1007/s11440-016-0468-2.

Chen, Yuanjiang, Jin Yin, and Yifu Hu. 2013. "Research on prestress quantitative loss law of soft rock slope anchor cable." *Chinese J Rock Mech Eng* 32 (8):1685-91.

Day, R. W. 1992. "Fill-Slope Failure and Repair." *J Perform Constr Fac* 6 (3):161-8. doi: 10.1061/(ASCE)0887-3828(1992)6:3(161).

Dickin, E. A. 1988. "Uplift Behavior of Horizontal Anchor Plates in Sand." *Journal of Geotechnical Engineering* 114 (11):1300-17.

Dickin, E. A., and M. Laman. 2007. "Uplift response of strip anchors in cohesionless soil." *Adv Eng Softw* 38 (8-9):618-25. doi: 10.1016/j.advengsoft.2006.08.041.

Dyson, A. S., and P. G. Rognon. 2014. "Pull-out capacity of tree root inspired anchors in shallow granular soils." *Geotech Lett* 4:301-5. doi: 10.1680/geolett.14.00061.

Eid, Hisham T., Ruslan S. Amarasinghe, Khaled H. Rabie, and Dharma Wijewickreme. 2015. "Residual shear strength of fine-grained soils and soil-solid interfaces at low effective normal

stresses." *Can Geotech J* 52 (2):198-210. doi: 10.1139/cgj-2014-0019.

Ersoy, Hakan, Murat Karahan, Kenan Gelisli, Aykut Akgun, Tugce Anilan, M. Oguz Sunnetci, and Bilgehan Kul Yahsi. 2019. "Modelling of the landslide-induced impulse waves in the Artvin Dam reservoir by empirical approach and 3D numerical simulation." *Eng Geol* 249:112-28. doi: 10.1016/j.enggeo.2018.12.025.

Evans, T. Matthew, and Nan Zhang. 2019. "Three-Dimensional Simulations of Plate Anchor Pullout in Granular Materials." *Int J Geomech* 19 (4). doi: 10.1061/(asce)gm.1943-5622.0001367.

Fu, Xiao, Wenyou Ji, Jianjing Zhang, Licong Cao, and Gang Fan. 2018. "Seismic response for plane sliding of slope reinforced by anchor-chain-framed ground beams through shaking table test." *Rock Soil Mech* 39 (5):1709-19.

GB 50007-2011. Code for design of building foundation. National Standard of the People's Republic of China. vol. 2011 (in Chinese).

GB 50021-2001. Code for investigation of geotechnical engineering. National Standard of the People's Republic of China. vol. 2001 (in Chinese).

GB/T 50123-2019. Standard for geotechnical testing method. National Standard of the People's Republic of China. vol. 2001 (in Chinese).

He, Manchao, Weili Gong, Jiong Wang, Peng Qi, Zhigang Tao, Shuai Du, and Yanyan Peng. 2014. "Development of a novel energy-absorbing bolt with extraordinarily large elongation and constant resistance." *Int J Rock Mech Min* 67:29-42. doi: 10.1016/j.ijrmms.2014.01.007.

Hejazi, Sayyed Mahdi, Mohammad Sheikhzadeh, Sayyed Mahdi Abtahi, and Ali Zadhoush. 2012. "A simple review of soil reinforcement by using natural and synthetic fibers." *Constr Build Mater* 30:100-16. doi: 10.1016/j.conbuildmat.2011.11.045.

Huang, Da, Pei-ji Li, and Duo-feng Cen. 2019. "A novel radial cable for restraining tensile failure in steep fill-rock interfaces." *J Mt Sci-Engl* 16 (7):1715-30. doi: 10.1007/s11629-018-5188-7.

Lajevardi, S. H., D. Dias, and J. Racinais. 2013. "Analysis of soil-welded steel mesh reinforcement interface interaction by pull-out tests." *Geotext Geomembranes* 40:48-57. doi: 10.1016/j.geotexmem.2013.08.002.

Li, Yanrong. 2013. "Effects of particle shape and size distribution on the shear strength behavior of composite soils." *B Eng Geol Environ* 72 (3-4):371-81. doi: 10.1007/s10064-013-0482-7.

Li, Zhe, Lei Sun, Lulu Liu, and Chenhui Guan. 2022. "Research on safety evaluation method of high-fill slope considering heterogeneity and anisotropy." *B Eng Geol Environ* 81 (7). doi: 10.1007/s10064-022-02766-0.

Liu, J., M. Liu, and Z. Zhu. 2012. "Sand Deformation around an Uplift Plate Anchor." *J Geotech Geoenviron* 138 (6):728-37. doi: 10.1061/(ASCE)GT.1943-5606.0000633.

Meyerhof, G. G., J. I. Adams. 1968. "The ultimate uplift capacity of foundations." *Can Geotech J* 5 (4):225–44. doi: 10.1139/t68-024.

Murao, Hidehiko, Kentaro Nakai, Toshihiro Noda, and Takahiro Yoshikawa. 2018. "Deformation-failure mechanism of saturated fill slopes due to resonance phenomena based on 1g shaking-table tests." *Can Geotech J* 55 (11):1668-81. doi: 10.1139/cgj-2017-0385.

Niroumand, H., and K. A. Kassim. 2013. "Pullout capacity of irregular shape anchor in sand." *Measurement* 46 (10):3876-82. doi: 10.1016/j.measurement.2013.07.042.

Rangari, Sunil M., Deepankar Choudhury, and D. M. Dewaikar. 2013. "Seismic uplift capacity of shallow horizontal strip anchor under oblique load using pseudo-dynamic approach." *Soils Found* 53 (5):692-707. doi: 10.1016/j.sandf.2013.08.007.

Sawwaf, Mae. 2007. "Behavior of strip footing on geogrid-reinforced sand over a soft clay slope." *Geotext Geomembranes* 25 (1):50-60. doi: 10.1016/j.geotexmem.2006.06.001.

Shi, Keyou, Xiaoping Wu, Ze Liu, and Shenglan Dai. 2019. "Coupled calculation model for anchoring force loss in a slope reinforced by a frame beam and anchor cables." *Eng Geol* 260. doi: 10.1016/j.enggeo.2019.105245.

Tilak, B. Vidya, and Narendra Kumar Samadhiya. 2021. "Pullout capacity of multi-plate horizontal anchors in sand: an experimental study." *Acta Geotech* 16 (9):2851-75. doi: 10.1007/s11440-021-01173-1.

Tong, L., L. Lian, and Y. Qiu. 2014. "Highway construction across heavily mined ground and steep topography in southern China." *B Eng Geol Environ* 73 (1):43-60. doi: 10.1007/s10064-013-0503-6.

Xie, Can, Shuchen Li, Shucai Li, Qikai Liao, and Shisen Zhao. 2017. "Study of anchorage force loss of anchor cable under seepage flow and soil creep." *Rock Soil Mech* 38 (8):2313-21,34. doi: 10.16285/j.rsm.2017.08.020.

Yan, Minjia, Yuanyou Xia, Tingting Liu, and Victor Mwango Bowa. 2019. "Limit analysis under seismic conditions of a slope reinforced with prestressed anchor cables." *Comput Geotech* 108:226-33. doi: 10.1016/j.compgeo.2018.12.027.

Yang, Guang Hua, Zhi-hui Zhong, Yu-cheng Zhang, and Xu-dong Fu. 2015. "Optimal design of anchor cables for slope reinforcement based on stress and displacement fields." *J Rock Mech Geotech* 7 (4):411-20. doi: 10.1016/j.jrmge.2015.04.004.

Yu, L., J. Liu, X. J. Kong, and Y. Hu. 2011. "Numerical study on plate anchor stability in clay." *Geotechnique* 61 (3):235-46. doi: 10.1680/geot.8.P.071.

Zhang, Guangcheng, Jiansong Tan, Lu Zhang, and Yong Xiang. 2015. "Linear regression analysis for factors influencing displacement of high-filled embankment slopes." *Geomech Eng* 8 (4):511-21. doi: 10.12989/gae.2015.8.4.511.

Zhang, Sheng, Xi Li, Jidong Teng, Xinyan Ma, and Daichao Sheng. 2017. "A theoretical method for determining sample mass in a sieving test." *Comput Geotech* 91:12-6. doi: 10.1016/j.compgeo.2017.06.004.

Zhao, Guoqing, Yuyou Yang, Haiqing Zhang, and Guolong Zhang. 2019. "A case study integrating field measurements and numerical analysis of high-fill slope stabilized with cast-in-place piles in Yunnan, China." *Eng Geol* 253:160-70. doi: 10.1016/j.enggeo.2019.03.005.

Zhou, Yanguo, Di Meng, Qiang Ma, Bo Huang, Daosheng Ling, and Yunmin Chen. 2019. "Centrifuge modeling of dynamic response of high fill slope by using generalized scaling law." *Eng Geol* 260. doi: 10.1016/j.enggeo.2019.105213.